

Interplay between Mechanochemical Patterning and Glassy Dynamics in Cellular Monolayers

Daniel Boocock¹,¹ Tsuyoshi Hirashima,^{2,3} and Edouard Hannezo^{1,*}

¹*Institute of Science and Technology Austria, Am Campus 1, 3400 Klosterneuburg, Austria*

²*Mechanobiology Institute, National University of Singapore, 5A Engineering Drive 1, 117411 Singapore*

³*Department of Physiology, Yong Loo Lin School of Medicine, National University of Singapore, Singapore*



(Received 20 March 2023; accepted 30 May 2023; published 20 July 2023)

Living tissues are characterized by an intrinsically mechanochemical interplay of active physical forces and complex biochemical signaling pathways. Either feature alone can give rise to complex emergent phenomena, for example, mechanically driven glassy dynamics and rigidity transitions, or chemically driven reaction-diffusion instabilities. An important question is how to quantitatively assess the contribution of these different cues to the large-scale dynamics of biological materials. We address this in Madin-Darby canine kidney (MDCK) monolayers, considering both mechanochemical feedback between extracellular signal-regulated kinase (ERK) signaling activity and cellular density as well as a mechanically active tissue rheology via a self-propelled vertex model. We show that the relative strength of active migration forces to mechanochemical couplings controls a transition from a uniform active glass to periodic spatiotemporal waves. We parametrize the model from published experimental data sets on MDCK monolayers and use it to make new predictions on the correlation functions of cellular dynamics and the dynamics of topological defects associated with the oscillatory phase of cells. Interestingly, MDCK monolayers are best described by an intermediary parameter region in which both mechanochemical couplings and noisy active propulsion have a strong influence on the dynamics. Finally, we study how tissue rheology and ERK waves produce feedback on one another and uncover a mechanism via which tissue fluidity can be controlled by mechanochemical waves at both the local and global levels.

DOI: [10.1103/PRXLife.1.013001](https://doi.org/10.1103/PRXLife.1.013001)

I. INTRODUCTION

Unraveling the properties of living materials requires an understanding of how active mechanical forces and material properties arise across subcellular and tissue scales, together with how these physical properties are integrated with complex biochemical signaling dynamics occurring within and between cells [1–3]. Experiments on *in vitro* monolayers have provided a fertile playground for developing and testing minimal active matter theories of supracellular dynamics, revealing features such as active nematic turbulence [4,5], glassy dynamics [6–9], unjamming transitions [10–12], and mechanical and/or chemical wave propagation [13–24]. So far these different phenomena have been studied largely in isolation from one another, often by employing a numerical framework such as active-particle [7] or vertex-based simulation [8]. A core generic feature within these models is the presence of local energy barriers linked to cell rearrangements (T1 transitions) which can be overcome by active motility forces, giving rise to active glass signatures for the spatiotemporal evolution of cellular velocity or density [9] that have

been compared and contrasted to the classical jamming and glass transitions from passive systems.

Another common feature in tissues is the presence of mechanochemical waves, which have been observed across multiple systems [25], for instance, as coupled waves of cell velocity, density, mechanical stress, and activation of the ERK/MAPK signaling pathway *in vitro* in Madin-Darby canine kidney (MDCK) cells [22,24]. Spatiotemporal ERK waves have also been observed and shown to be critical *in vivo* for bone regeneration in zebrafish [26], murine cochlear morphogenesis [27], and murine skin wound healing [28]. Recently in [24] we proposed a minimal quantitative one-dimensional model showing how such waves can arise from simple mechanochemical couplings [Figs. 1(a) and 1(b)] via a spatiotemporal instability that can recapitulate a number of mean-field features of wave propagation [22,24]. However, how to unify this mechanochemical description with previous modeling and experimental observations of the jamming transitions and glassy dynamics in cell monolayers remains an outstanding challenge.

In this work we implement a numerical model for the rheology of an active two-dimensional (2D) confluent tissue, a self-propelled vertex model, that also incorporates mechanochemical feedback between ERK signaling dynamics and cellular density. We show that the relative strength of active migration forces to oscillatory mechanochemical couplings controls a transition from a uniform active glass to one with periodic spatiotemporal patterns. By identifying relationships between mechanochemical coupling parameters and oscillatory amplitudes of ERK and density, we are able

*edouard.hannezo@ist.ac.at

Published by the American Physical Society under the terms of the [Creative Commons Attribution 4.0 International](https://creativecommons.org/licenses/by/4.0/) license. Further distribution of this work must maintain attribution to the author(s) and the published article's title, journal citation, and DOI.

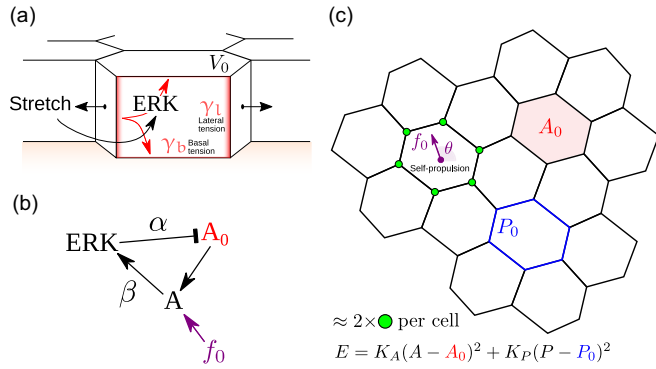


FIG. 1. (a) Schematic of the three-dimensional forces exerted on cells in confluent monolayers. The in-plane cell area is determined by a balance of cytoskeletal forces on the basal and lateral sides, which can be modulated by ERK signaling activity [22,24]. (b) Schematic of the mechanochemical couplings considered in the model. The ERK signaling activity impacts on preferred cell area A_0 with coupling strength α , creating mechanical stresses for cells with area A below or above this preferred value. This, together with stresses from self-propulsion forces f_0 , results in changes in area A which feeds back on ERK with coupling strength β . (c) Schematic of the in-plane 2D vertex model, its associated energy, and persistent random motility forces f_0 .

to parametrize the model from published experimental data sets on MDCK monolayers *in vitro* [22,24]. We show that a number of quantitative features, including temporal auto-correlation functions and the dynamics of topological defects associated with the mechanochemical phase of cells, are recapitulated in an intermediary parameter region where both ERK-density oscillations and noisy active propulsion play an important role. Finally, we study computationally how the T1 transition frequency, and thus local tissue fluidity, is subject to spatiotemporal control by oscillatory mechanochemical activity, investigate the effect of mechanochemical waves on global tissue fluidization, and discuss the relevance of this model to other biological settings.

II. RESULTS

A. Active vertex model with mechanochemical feedback

We start by considering the typical vertex model energy, which provides a minimal description for a confluent epithelial monolayer by assuming that 2D cell shapes arise from a balance between adhesive and tensile forces at the cell-cell contacts [10,29–31]

$$E = \sum_i K_A (A^i - A_0^i)^2 + K_P (P^i - P_0^i)^2, \quad (1)$$

where the first term on the right-hand side models a target cellular area A_0^i and the second term assumes that cells have a preferred perimeter P_0^i based on a balance between cell-cell adhesion and cytoskeletal driven tension [Fig. 1(c)]. A more mathematical viewpoint considers this preferred perimeter as the first nonlinear stabilizing terms allowed by symmetry. An important result concerns the value of the shape index $p_0 = P_0/\sqrt{A_0}$, which in homogeneous systems controls the

tissue fluidity [10]: Systems with $p_0 \lesssim 3.81$ are in a solid state characterized by energy barriers for cell rearrangements and systems with $p_0 \gtrsim 3.81$ are in a fluid state where rigidity is lost. To implement the dynamics of this model numerically, we used the cell-based CHASTE library [32] to develop a mechanochemically coupled vertex model. The motion of tricellular junctions \vec{r}_i was described by overdamped dynamics $\zeta \partial_t \vec{r}_i = \vec{F}_i$, where the timescale of stress propagation is affected by a friction coefficient ζ with the substrate and the force \vec{F}_i derives from the vertex model energy described above.

Although investigations of the vertex model have concentrated mostly on monolayers constituting cells with constant mechanical properties and self-propulsion, some works have started to investigate the effect of additional variables such as biochemical signaling, morphogen diffusion, or mechanosensation [33–35]. Here we incorporate and study the effect of mesoscopic oscillatory dynamics using mechanochemical ERK waves as a basis. To do so we generalize our previous one-dimensional mechanochemical model [24] to 2D cells with target areas A_0^i dependent on local ERK signaling activity E_i with delay τ_A [Figs. 1(a) and 1(b)],

$$\tau_A \partial_t A_0^i = (1 - A_0^i) - \alpha E_i, \quad (2)$$

where α is a coupling strength that controls how much ERK signaling impacts on the preferred cell area A_0 (i.e., signaling to mechanics) and has been shown to be positive in optogenetic ERK activation experiments [24]. Here and in the following we nondimensionalize length scales by the average cell area $\langle A \rangle$ ($\vec{r}_i \leftarrow \vec{r}_i/\sqrt{\langle A \rangle}$) and center ERK activity by its steady-state activation E_0 ($E_i \leftarrow E_i - E_0$) (see vertex model simulations in [36] for details). An additional equation on ERK activity is required to close the system, which, based on previous experimental findings [22,24], we take as proportional to the local area A_i with a delay τ_E ,

$$\tau_E \partial_t E_i = -E_i - E_i^3 + \beta (A^i - 1), \quad (3)$$

where β is a coupling strength that controls the sensitivity of ERK activation as a function of cell area (i.e., mechanics to signaling) and has been shown to also be positive in monolayer stretching experiments [22]. The cubic term in the ERK activity equation ensures nonlinear stability of simulations. Together these equations describe generic lowest-order couplings around a nondimensional steady state of $A^i = A_0^i = 1$ and $E_i = 0$. This 2D model is identical at linear order to the 1D model studied analytically in [24] and leads to spatiotemporal instabilities for a critical value of the product of mechanochemical couplings $(\alpha\beta)_c$ (see Fig. S1 in [36] for details). Physically, this arises due to an oscillatory instability in a feedback loop in which changes in actual area A^i are mechanosensed via ERK signaling to modify target areas A_0^i , with energy minimization closing A_0^i back onto A^i . The core role of feedback between ERK activity and cellular density is consistent with the experimental observation that cellular density waves are abrogated upon ERK inhibition [22]. To constrain parameters, we take the timescales τ_A and τ_E as previously inferred [24] and the ratio K_A/K_P from the literature [9,37] and leave the ratio of elasticity to substrate friction $K_{A,P}/\zeta$ as a free parameter in order to match the wavelength in data (approximately 20 cells; see Table S1 in [36]). Running

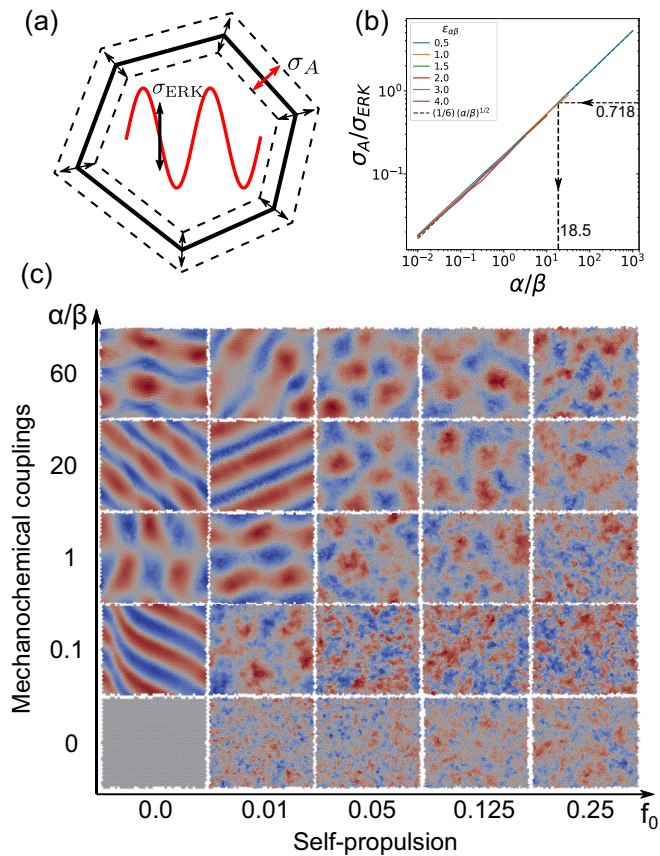


FIG. 2. (a) and (b) Relative amplitude of area to ERK oscillation σ_A/σ_{ERK} vs ratio of mechanochemical coupling constants α/β , showing that different values of the product $\alpha\beta$ robustly scale along the same master curve, allowing us to fit α/β from the experimentally observed value of σ_A/σ_{ERK} (dashed lines; see also Fig. S3B in [36]). (c) Phase diagram of mechanochemical patterning in a 2D vertex model with ERK signaling activity and self-propulsion, as a function of active self-propulsion forces f_0 (which introduce persistent noise in the system) and the relative strength of mechanical and chemical couplings α/β (see Fig. S4 in [36]) for a phase diagram as a function of the product $\alpha\beta$).

simulations for different values of the coupling constants α and β confirm the predictions from linear stability that regular spatiotemporal waves emerge above a critical value of $\alpha\beta$ (Figs. S1A and S1B in [36], which depend on the shape index p_0) whereas different ratios of α/β dictate the relative amplitudes of mechanical over ERK activity waves [Figs. 2(a) and 2(b)]. In summary, α and β are independent parameters, each quantifying one side of the mechanochemical feedback loop between mechanics and ERK activity, with their product and ratio controlling different key aspects of the resulting dynamics. While the threshold of the instability depends only on the product $\alpha\beta$, whether this instability is most prominent in terms of amplitude of area or ERK oscillations is dictated by the ratio α/β .

To compare features more quantitatively with data, we seek to use these findings to better constrain parameters α and β . Simulating with different values of α and β and calculating the amplitudes of area and ERK oscillations (σ_A and σ_E , respectively) show that σ_A/σ_E scales with the ratio

of α/β , independent of the value of $\alpha\beta$, so that all tested values of $\alpha\beta$ could be rescaled for the power law $\sigma_A/\sigma_E \propto (\alpha/\beta)^{1/2}$ [Fig. 2(b)]. Given that σ_A/σ_E is highly consistent over the three repeats of previously published data sets on mechanochemical ERK patterning in confluent MDCK monolayers [24] (Fig. S3B in [36]), this provides a robust method for constraining α/β , which yields $\alpha/\beta \approx 18.5$ [Fig. 2(b)]. We delay the remaining parametrization of the product $\alpha\beta$ until we introduce active cell migration to our model, as it affects individual amplitudes σ_A and σ_E (Figs. S3D–S3F in [36]), while the parametrization of α/β described above remains robust (Fig. S3C in [36]).

Despite our parametrization being able to match several qualitative features and summary statistics of the data (Figs. S1C, S2B, and S2C in [36]), visual comparisons to experimental data sets [Fig. 2(c)] make it clear that ERK waves in MDCK monolayers are much more disordered than the ones we expect for this minimal model in the noise-free limit. Although a number of sources of noise could be considered, ranging from noise in ERK signaling to junctional fluctuations, previous modeling [9] has shown that a number of features of MDCK collective dynamics can be explained by a model of glassy dynamics driven by noisy active migration forces. Thus, in addition to the mechanochemical model above, we consider active cell migration in direction \vec{p}_i (unit vector) with characteristic force f_0 [8,38]. As a result, the total force exerted by cells on the substrate (traction force) has a contribution from active self-propulsion $-f_0\vec{p}_i$ as well as a frictional component $\zeta\partial_t\vec{r}_i$ [16]. Writing the force balance on cell centers \vec{r}_i thus gives

$$\zeta\partial_t\vec{r}_i = \vec{F}_i + f_0\vec{p}_i, \quad (4)$$

where the angle of polarization θ_i of the polarity unit vector \vec{p}_i evolves with zero-mean Gaussian white noise as $\partial_t\theta_i = \eta_i(t)$, giving a cellular persistence time $\tau_p = 2/\langle\eta_i^2\rangle$. This is the characteristic time at which polarity evolves due to fluctuations or external perturbations. Based on published data on the timescale of traction force changes upon optogenetic perturbation [22], we can constrain $\tau_p = 30$ min (see vertex model simulations in [36] for more details). In practice, the self-propulsion force always appears with substrate friction as the ratio f_0/ζ , which we simply refer to as f_0 in the rest of this paper. In the vertex model implementation, the propulsion force for each cell is applied to all of the vertices defining its tricellular junctions.

B. Effect of self-propulsion and mechanochemical couplings on monolayer dynamics

In the absence of mechanochemical couplings $\alpha = 0$ (where we keep $\beta \neq 0$ so that ERK signaling is a passive variable that tracks cell area), we find, as expected from classical work [8], that a solid monolayer $p_0 \lesssim 3.81$ can be fluidized by active traction forces above a critical value f_0 (Fig. S1D in [36] and Movie S1), leading to collective streaming and locally disordered cellular shapes characteristic of glassy dynamics [8,9]. However, in this $\alpha = 0$ case, ERK signaling does not show any spatial or temporal periodicity (Fig. S2A in [36]; see also [37]), irrespective of whether f_0 is above or below the unjamming threshold, which contrasts with

experimental observations of ERK patterning [22,24]. Thus, the experimental dynamics does not fully match the cases of active jamming or oscillatory mechanochemical signaling alone and we hypothesize that the system might be better described by a combination of the two phenomena.

To test this, we first explore the phase diagram of possible patterns in ERK signaling and cell area for different values of α , β , and f_0 (Fig. S4 in [36]). As expected, stronger mechanochemical couplings $\alpha\beta$ favor periodic instabilities while large random migration forces f_0 favor noisy glasslike dynamics with unstructured ERK patterns. Furthermore, we also find that larger ratios α/β favor periodic patterning [Fig. 2(c)]; this is because larger α/β increases the relative amplitude of area to ERK oscillations, which makes the system more resistant to area perturbations induced by migration forces.

We then repeat our analysis of ERK and area amplitudes for fitting mechanochemical couplings α and β in the presence of self-propulsion noise f_0 , finding that our previous estimate for α/β from amplitude ratio σ_A/σ_E was quite robust to different values of f_0 (Figs. S3C and S3F in [36]). Furthermore, by jointly matching amplitudes from σ_A , σ_E , and σ_A/σ_E , we could estimate a region of parameter space $\epsilon_{\alpha\beta} = (\alpha\beta - \alpha\beta_c)/\alpha\beta_c \approx 0.8$ and $f_0 = 0.125\text{--}0.15$ where our model is fully parametrized from data (Figs. S3D and S3F in [36] and simulation in Movie S1). This quantitative analysis of amplitudes, along with qualitative inspection of simulations, suggests that intermediate values of α/β and f_0 could match experimental data sets.

C. Quantitative comparisons between simulations and MDCK experiments

To confirm this, we seek to perform further quantitative spatiotemporal analysis of the mechanochemical patterns formed across different conditions. Inspired by a previous analysis of subcellular biochemical waves in starfish egg cells [39], we take advantage of the periodicity of ERK signaling to define a phase ϕ for the oscillation in every cell (Fig. S7 in [36]), which could be mapped spatially and temporally across the entire tissue [Figs. 3(a)–3(c)]. We then study the effect of different types of activity on the patterns by tracking the motion and creation-annihilation dynamics of ± 1 vortex defects corresponding to singularities in the phase (see Movies S2–S4 and the Supplemental Material [36] for details on the methods [40,41]), which provide a simpler metric to characterize the complex two-dimensional patterns of ERK activity.

We find that the dynamics of the topological defects is markedly different for different values of our parameters. While for all parameter values the distribution of defect lifetimes is well fitted by an exponential (as in [39]), the average lifetime is strongly dependent on both the mechanochemical coupling strengths α and β and migration force f_0 [Fig. 3(e) and Fig. S5A in [36]] with higher f_0 resulting in higher effective diffusion of topological defects and thus higher probability of defect annihilation. On the other hand, higher overall mechanochemical coupling strength $\alpha\beta$ [Fig. 3(e)] or coupling ratio α/β (Fig. S5A in [36]) favor regular oscillations which translate into more regular motion of defects and longer lifetimes. Strikingly, returning to the experimental data, we

find that the predicted exponential scaling provides a good fit for the experimental defect lifetime distribution [Fig. 3(d)]. Furthermore, by comparing the predicted and experimentally observed average lifetimes, we find good agreement, thus independently validating our estimates of f_0 , α , and β [Fig. 3(e)]. This provides additional evidence that the data are consistent with a mixed regime of active glassy dynamics and mechanochemical patterning.

Next we reason that the decay in the temporal autocorrelation of ERK signaling could be used as an additional test of the model. Indeed, as expected from visual inspection of our simulations [Fig. 2(c), first column], the noise-free limit displays highly periodic autocorrelation functions with little decay (Fig. S2B in [36]), which could be quantified by the amplitude of the first maximum [Figs. 3(f)–3(h)]. Increasing migration noise f_0 results in a gradual loss of periodicity, with a related decay in the amplitude of the first peak. When compared to data, self-propulsion values in the range $f_0 = 0.2\text{--}0.25$ could explain the experimental correlation, a somewhat higher value than inferred from other metrics, which could be due to simulations considering only a single source of noise (persistent random migration), whereas others such as cell-cell heterogeneity and cell divisions could be present experimentally.

D. Mechanochemical wave modulation of the global and local fluidity of the tissue

Finally, we wish to understand theoretically how the solid or fluid state of the monolayer affects mechanochemical waves in the absence of self-propulsion, i.e., for $f_0 = 0$. We simulate over a range of $\alpha\beta$ different values of the preferred cell perimeter $p_0 = 3.5\text{--}3.9$, finding that solidification leads to a later onset of instability but otherwise qualitatively the same collective mechanochemical oscillations (Figs. S1A–S1C in [36]). This implies that ERK mechanochemical patterning is fairly robust to the rheological state of monolayers, which is likely due to the fact that ERK is only coupled to the local density of cells, something strongly constrained by the confluent assumption of the vertex model.

However, we reason that changes in cellular areas and velocities created by mechanochemical waves might provide feedback on the fluidlike or solidlike material properties of the monolayer, for instance, by locally changing or overcoming the energy barriers related to topological T1 rearrangements. To test this, we return to the solid regime $p_0 = 3.5\text{--}3.8$, which is fluidized by critical values of f_0 (Figs. S6A and S6B in [36]) as previously described [8]. We then examine whether values of mechanochemical couplings $\alpha\beta$ might modify the threshold of fluidization or unjamming. We find that the mean square displacement (MSD) of cells increases with increasing values of $\alpha\beta$ (Figs. S6E and S6F in [36]). To test this, we perform ERK inhibition experiments and confirm that this results in decreased MSD compared to control (Fig. S6D in [36]). From a theoretical perspective, this supports the idea that mechanochemical waves provide an additional source of effective noise, decreasing the threshold of motility force f_0 required for T1 transitions and unjamming, an effect which is amplified for the lower value of $p_0 = 3.5$ (Fig. S6 in [36]).

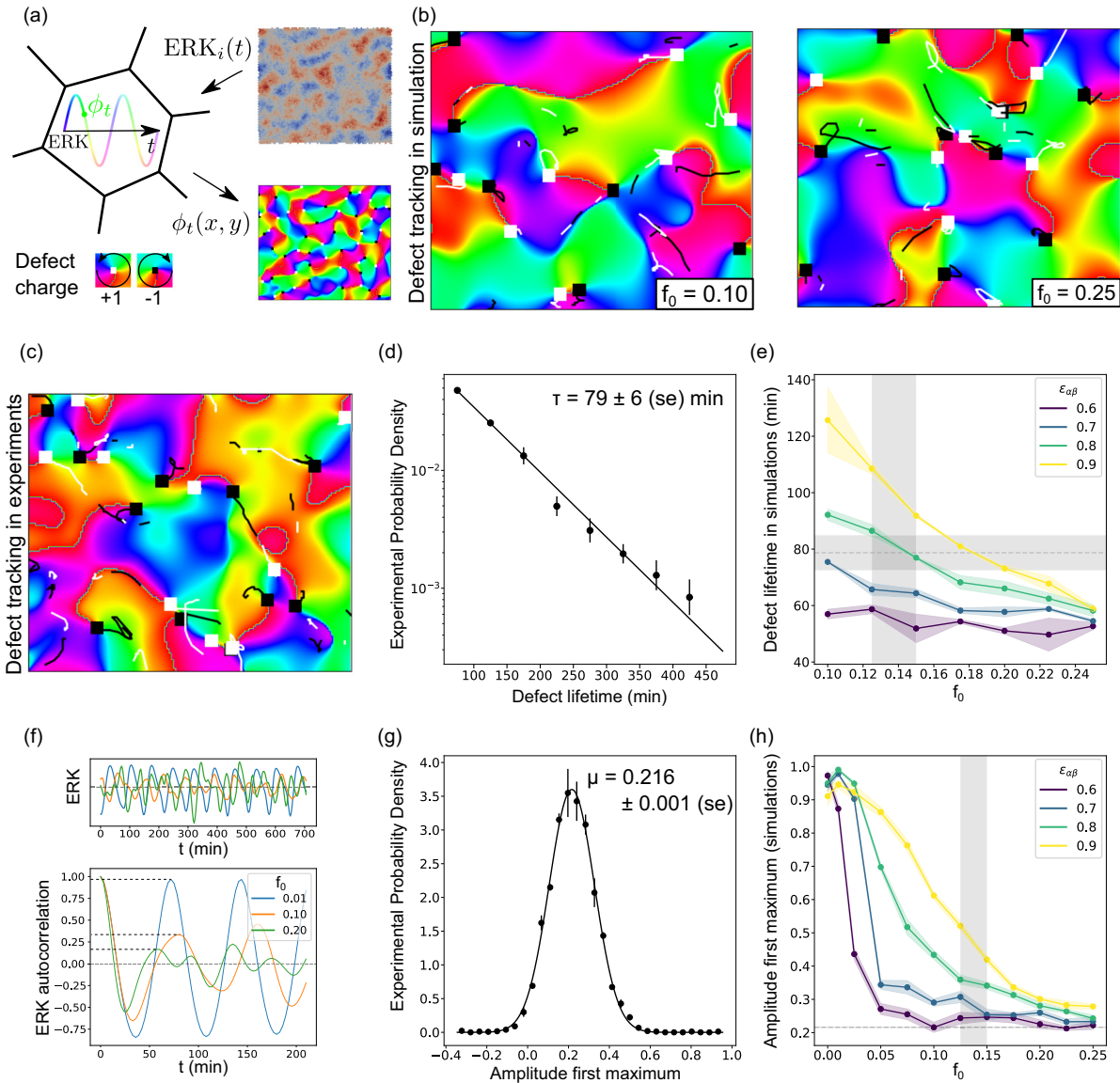


FIG. 3. (a) Overview of the tissue-level analysis of ERK patterning. Local cellular phases of ERK signaling activity are smoothed into continuous fields containing \pm topological defects. (b) Phase field of ERK activity (color coded for phase), for different values of active self-propulsion f_0 together with the identification and tracking in time of topological defects (white and black squares indicate $+1$ and -1 charges, respectively). (c) Phase field of ERK activity in MDCK monolayers, with the same analysis as in (b). (d) Experimental lifetime of ERK phase topological defects in MDCK monolayers, showing a good fit to an exponential distribution as observed in simulations. (e) Average lifetime of ERK phase topological defects in the simulations as a function of active self-propulsion f_0 , for different values of mechanochemical coupling strength $\epsilon_{\alpha\beta} = (\alpha\beta - \alpha\beta_c)/\alpha\beta_c$. Shaded intervals indicate experimental values of mean defect lifetime and estimates of f_0 , showing that model values of $\epsilon_{\alpha\beta} \approx 0.8$ and $f_0 = 0.125\text{--}1.5$ explain the experimental lifetime data while also being consistent with predictions of α , β , and f_0 from ERK and area amplitudes (Figs. S3D–S3F in [36]). (f) Representative tracks of ERK dynamics in the simulations for different values of f_0 (top) together with corresponding autocorrelation functions (bottom), showing that larger active self-propulsion noise (larger f_0) causes rapid decays, as quantified by the amplitude of the first peak (dashed horizontal lines). (g) Distribution of first-peak amplitudes of ERK autocorrelation across MDCK cells (with fit to normal distribution, see the Supplemental Material [36] for details). (h) First-peak amplitude of the ERK autocorrelation in simulations as a function of active self-propulsion f_0 and mechanochemical couplings $\epsilon_{\alpha\beta}$. Shaded intervals indicate estimates of f_0 as in (e) and the experimental measurement of first-peak amplitude from (g).

Furthermore, we find that the timing and location of T1 transitions are strongly affected by the local phase of mechanochemical waves. By calculating the probability of T1 transitions as a function of the ERK phase ϕ , we indeed observe a twofold to threefold change in the frequency of topological rearrangements between low and high ERK states

[Fig. 4(b)], which is robust to changes in migration forces f_0 . This can be rationalized by considering that the area and ERK are closely temporally correlated (ERK lagging slightly behind area with timescale τ_E) so that low ERK states are also low-area states with low target area and correspondingly high shape index ($p_0 = P_0/\sqrt{A_0}$). Thus, these regions have higher

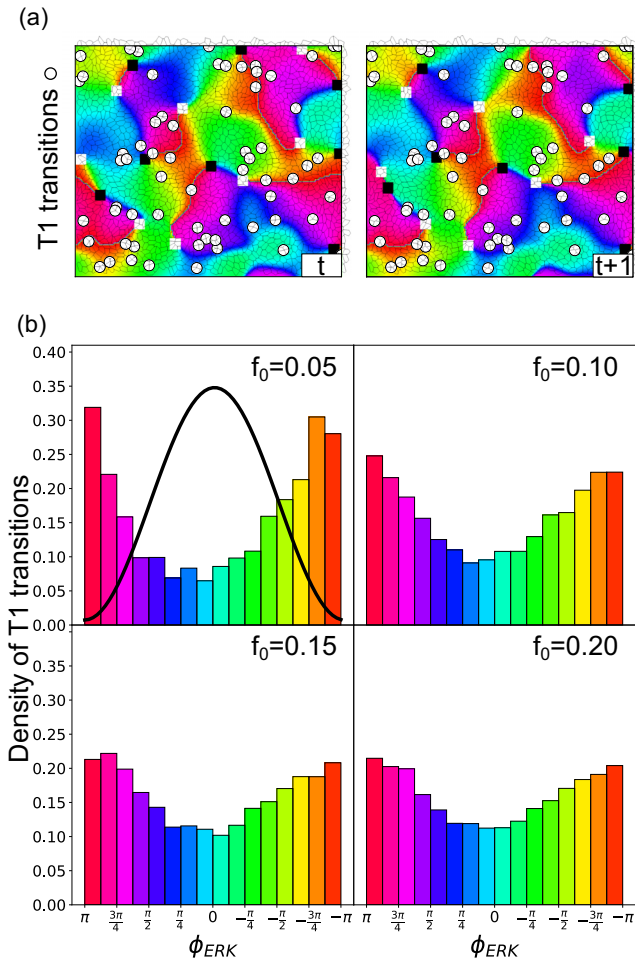


FIG. 4. (a) Representative snapshots for the mapping of cell-cell rearrangements (T1 transitions, white circles) to local ERK activity (or phase; see Fig. S7 in [36] for color code) in vertex-model simulations. (b) Distribution of T1 transition probability as a function of ERK phase, for different values of active self-propulsion force f_0 , showing strong anticorrelation with ERK activity (the black curve shows absolute value and color shows phase) and T1 transitions.

geometric incompatibility (or frustration) [10] and a propensity towards T1 transitions. The result is that ERK waves can drive local cycles of fluidization and solidification in the monolayer with material properties controlled via patterns of signaling.

III. DISCUSSION

In this work we have explored the interplay between tissue mechanics and biochemical signaling in a minimal two-dimensional vertex model of a confluent monolayer. Vertex models have been extensively used in the past few years as minimal descriptions of 2D and 3D tissue organization, identifying in particular key geometrical signatures of rigidity transitions, both in the absence of noise and with active self-propulsion forces [8,10,29,42,43]. In the latter case, the models make specific predictions about glassy dynamics which have common and divergent features compared to the classical glass transition. Interestingly, a number of signatures

of active glassy dynamics appear conserved across different modeling frameworks (e.g., vertex vs particle-based models) [7–9]; however, these models have historically concentrated on either tissues formed from a single cell type [10,42] or the demixing of two cell types possessing constant and defined mechanical properties [44–46].

Here we have considered a model which combines a glassy rheology with an emergent patterning phenomenon that specifies spatiotemporally varying mechanical properties across a tissue. More specifically, we have considered cells with both active self-propulsion and ERK-density mechanochemical couplings, by associating with each cell a temporally fluctuating signaling activity and bidirectionally coupling this activity to local cellular mechanics. We concentrated on ERK/MAPK signaling, as this is a key pathway for force sensing, force generation, and a number of key cellular processes [47–55] (e.g., migration, contractility, differentiation, and apoptosis) and because previous works in MDCK monolayers have dissected the types of mechanochemical couplings that give rise to waves of ERK activity and cell density [22,24]. However, how to characterize in two dimensions the complex spatiotemporal patterns observed experimentally was not clear. The simulation framework that we proposed here, as well as the associated quantitative analysis based on oscillatory amplitudes, topological defects, and autocorrelation functions, has allowed us to characterize this system and is highly general to any pathway which forms spatiotemporal patterns by interacting with cellular mechanics, for instance, YAP or TAZ [18]. From a more theoretical point of view, this provides an example of pulsating active matter, which has been recently explored via particle-based simulations with oscillating radii and continuum theory [56]. Systematically comparing predictions of our findings to different implementations of tissues, such as particle-based models [56] or phase-field models [57], with distinct rheological properties would be an interesting next step.

Exploring the phase space of possible patterning instabilities revealed a number of interesting features. While the relative strength of biochemical-to-mechanical vs mechanical-to-biochemical coupling (α/β) plays a key role in determining the relative amplitude of ERK vs cell density oscillations, the ratio of self-propulsion forces f_0 to both global mechanochemical coupling strength $\alpha\beta$ and the mechanochemical coupling ratio α/β determines whether the system is closer to a uniform active glass or a periodic patterning state. Interestingly, we found that multiple signatures of the data, including amplitudes of biochemical and mechanical oscillations, the dynamics of topological defects in the phase of ERK signaling, and the decay in autocorrelation of ERK signaling, are consistent with MDCK monolayers being in an intermediate regime characterized by a combination of ERK-density waves and noisy active migration, providing a potentially unifying framework to previous modeling of these types of dynamics [6,9,24].

In the future, it will be interesting to test the role of additional sources of fluctuations in addition to cell migration, for instance, in ERK signaling dynamics itself or on cell mechanics (i.e., shape index, junctional tensions [58], or average cell density), as well as the effect of time-independent cell heterogeneity (i.e., in active migration force [59] or in

proliferation-dependent cell size [60]). Other interesting directions would be to incorporate the effect of active nematics and turbulence [61–65] or to consider alternative theoretical modes of mechanosensitive couplings which have been recently proposed, for instance, on junctional tensions driving active cell rearrangements [34] or junction remodeling [34,66,67]. Finally, while we have considered a minimal model of ERK dynamics and its coupling to mechanics, considering more complex features of the pathway such as activator-inhibitor dynamics [68] would be an important next step.

IV. MATERIALS AND METHODS

Code to run vertex model simulations was built using the CHASTE library [32] and is available for download from [69]. Analysis was performed using custom codes in PYTHON that are linked to from the GitHub repository. Additional code and data are available upon request. Details of the numerical

procedure, parameter fitting, and quantification strategy can be found in Supplemental Material [36].

ACKNOWLEDGMENTS

We thank all members of the Hannezo group for discussions and suggestions, as well as Sound Wai Phow for technical assistance. This work received funding from the European Research Council under the EU Horizon 2020 research and innovation program Grant Agreement No. 851288 (E.H.), JSPS KAKENHI Grant No. 21H05290, and the Ministry of Education under the Research Centres of Excellence program through the MBI at NUS.

D.B. and E.H. conceptualized the work; D.B. performed the simulations; T.H. conducted the experiments; D.B. and T.H. performed analysis; E.H. and D.B. wrote the manuscript; and all authors edited the manuscript.

The authors declare no competing financial interests.

-
- [1] M. C. Marchetti, J.-F. Joanny, S. Ramaswamy, T. B. Liverpool, J. Prost, M. Rao, and R. A. Simha, Hydrodynamics of soft active matter, *Rev. Mod. Phys.* **85**, 1143 (2013).
- [2] E. Hannezo and C.-P. Heisenberg, Mechanochemical feedback loops in development and disease, *Cell* **178**, 12 (2019).
- [3] P.-F. Lenne, E. Munro, I. Heemskerk, A. Warmflash, Laura Bocanegra-Moreno, K. Kishi, A. Kicheva, Y. Long, A. Fruleux, A. Boudaoud *et al.*, Roadmap for the multiscale coupling of biochemical and mechanical signals during development, *Phys. Biol.* **18**, 041501 (2021).
- [4] A. Doostmohammadi, J. Ignés-Mullol, J. M. Yeomans, and F. Sagués, Active nematics, *Nat. Commun.* **9**, 3246 (2018).
- [5] R. Alert, J. Casademunt, and J.-F. Joanny, Active turbulence, *Annu. Rev. Condens. Matter Phys.* **13**, 143 (2022).
- [6] T. E. Angelini, E. Hannezo, X. Trepate, M. Marquez, J. J. Fredberg, and D. A. Weitz, Glass-like dynamics of collective cell migration, *Proc. Natl. Acad. Sci. USA* **108**, 4714 (2011).
- [7] S. Garcia, E. Hannezo, J. Elgeti, J.-F. Joanny, P. Silberzan, and N. S. Gov, Physics of active jamming during collective cellular motion in a monolayer, *Proc. Natl. Acad. Sci. USA* **112**, 15314 (2015).
- [8] D. Bi, X. Yang, M. C. Marchetti, and M. L. Manning, Motility-Driven Glass and Jamming Transitions in Biological Tissues, *Phys. Rev. X* **6**, 021011 (2016).
- [9] S. Henkes, K. Kostanjevec, J. M. Collinson, R. Sknepnek, and E. Bertin, Dense active matter model of motion patterns in confluent cell monolayers, *Nat. Commun.* **11**, 1405 (2020).
- [10] D. Bi, J. H. Lopez, J. M. Schwarz, and M. L. Manning, A density-independent rigidity transition in biological tissues, *Nat. Phys.* **11**, 1074 (2015).
- [11] J.-A. Park, J. H. Kim, D. Bi, J. A. Mitchel, N. T. Qazvini, K. Tantisira, C. Y. Park, M. McGill, S.-H. Kim, B. Gweon *et al.*, Unjamming and cell shape in the asthmatic airway epithelium, *Nat. Mater.* **14**, 1040 (2015).
- [12] C. Malinverno, S. Corallino, F. Giavazzi, M. Bergert, Q. Li, M. Leoni, A. Disanza, E. Frittoli, A. Oldani, E. Martini *et al.*, Endocytic reawakening of motility in jammed epithelia, *Nat. Mater.* **16**, 587 (2017).
- [13] X. Serra-Picamal, V. Conte, R. Vincent, E. Anon, D. T. Tambe, E. Bazellieres, J. P. Butler, J. J. Fredberg, and X. Trepate, Mechanical waves during tissue expansion, *Nat. Phys.* **8**, 628 (2012).
- [14] A. Zaritsky, D. Kaplan, I. Hecht, S. Natan, L. Wolf, N. S. Gov, E. Ben-Jacob, and I. Tsarfaty, Propagating waves of directionality and coordination orchestrate collective cell migration, *PLoS Comput. Biol.* **10**, e1003747 (2014).
- [15] S. Banerjee, K. J. C. Utuje, and M. C. Marchetti, Propagating Stress Waves During Epithelial Expansion, *Phys. Rev. Lett.* **114**, 228101 (2015).
- [16] J. Notbohm, S. Banerjee, K. J. C. Utuje, B. Gweon, H. Jang, Y. Park, J. Shin, J. P. Butler, J. J. Fredberg, and M. C. Marchetti, Cellular contraction and polarization drive collective cellular motion, *Biophys. J.* **110**, 2729 (2016).
- [17] S. Tlili, E. Gauquelin, B. Li, O. Cardoso, B. Ladoux, H. Delanoë-Ayari, and F. Graner, Collective cell migration without proliferation: Density determines cell velocity and wave velocity, *R. Soc. Open Sci.* **5**, 172421 (2018).
- [18] G. Peyret, R. Mueller, J. d'Alessandro, S. Begnaud, P. Marcq, R.-M. Mège, J. M. Yeomans, A. Doostmohammadi, and B. Ladoux, Sustained oscillations of epithelial cell sheets, *Biophys. J.* **117**, 464 (2019).
- [19] V. Petrolli, M. L. Goff, M. Tadrous, K. Martens, C. Allier, O. Mandula, L. Hervé, S. Henkes, R. Sknepnek, T. Boudou *et al.*, Confinement-Induced Transition between Wavelike Collective Cell Migration Modes, *Phys. Rev. Lett.* **122**, 168101 (2019).
- [20] K. Aoki, Y. Kondo, H. Naoki, T. Hiratsuka, R. E. Itoh, and M. Matsuda, Propagating wave of ERK activation orients collective cell migration, *Dev. Cell* **43**, 305 (2017).
- [21] S.-Z. Lin, B. Li, G. Lan, and X.-Q. Feng, Activation and synchronization of the oscillatory morphodynamics in multicellular monolayer, *Proc. Natl. Acad. Sci. USA* **114**, 8157 (2017).
- [22] N. Hino, L. Rossetti, A. Marín-Llauradó, K. Aoki, X. Trepate, M. Matsuda, and T. Hirashima, ERK-mediated mechanochemical waves direct collective cell polarization, *Dev. Cell* **53**, 646 (2020).

- [23] Y. Asakura, Y. Kondo, K. Aoki, and H. Naoki, Hierarchical modeling of mechano-chemical dynamics of epithelial sheets across cells and tissue, *Sci. Rep.* **11**, 4069 (2021).
- [24] D. Boocock, N. Hino, N. Ruzickova, T. Hirashima, and E. Hannezo, Theory of mechanochemical patterning and optimal migration in cell monolayers, *Nat. Phys.* **17**, 267 (2021).
- [25] S. Armon, M. S. Bull, A. Aranda-Diaz, and M. Prakash, Ultrafast epithelial contractions provide insights into contraction speed limits and tissue integrity, *Proc. Natl. Acad. Sci. USA* **115**, E10333 (2018).
- [26] A. De Simone, M. N. Evanitsky, L. Hayden, B. D. Cox, J. Wang, V. A. Tornini, J. Ou, A. Chao, K. D. Poss, and S. Di Talia, Control of osteoblast regeneration by a train of erk activity waves, *Nature (London)* **590**, 129 (2021).
- [27] M. Ishii, T. Tateya, M. Matsuda, and T. Hirashima, Retrograde ERK activation waves drive base-to-apex multicellular flow in murine cochlear duct morphogenesis, *eLife* **10**, e61092 (2021).
- [28] T. Hiratsuka, Y. Fujita, H. Naoki, K. Aoki, Y. Kamioka, and M. Matsuda, Intercellular propagation of extracellular signal-regulated kinase activation revealed by in vivo imaging of mouse skin, *eLife* **4**, e05178 (2015).
- [29] R. Farhadifar, J.-C. Röper, B. Aigouy, S. Eaton, and F. Jülicher, The influence of cell mechanics, cell-cell interactions, and proliferation on epithelial packing, *Curr. Biol.* **17**, 2095 (2007).
- [30] E. Hannezo, J. Prost, and J.-F. Joanny, Theory of epithelial sheet morphology in three dimensions, *Proc. Natl. Acad. Sci. USA* **111**, 27 (2014).
- [31] S. Alt, P. Ganguly, and G. Salbreux, Vertex models: From cell mechanics to tissue morphogenesis, *Philos. Trans. R. Soc. B* **372**, 20150520 (2017).
- [32] F. R. Cooper, R. E. Baker, M. O. Bernabeu, R. Bordas, L. Bowler, A. Bueno-Orovio, H. M. Byrne, V. Carapella, L. Cardone-Noott, J. Cooper *et al.*, Chaste: Cancer, heart and soft tissue environment, *J. Open Source Softw.* **5**, 1848 (2020).
- [33] S. Okuda, T. Miura, Y. Inoue, T. Adachi, and M. Eiraku, Combining turing and 3D vertex models reproduces autonomous multicellular morphogenesis with undulation, tubulation, and branching, *Sci. Rep.* **8**, 2386 (2018).
- [34] R. Sknepnek, I. Djafer-Cherif, M. Chuai, C. J. Weijer, and S. Henkes, Generating active T1 transitions through mechanochemical feedback, *eLife* **12**, e79862 (2023).
- [35] R. Cohen, S. Taiber, O. Loza, S. Kasirer, S. Woland, and D. Sprinzak, Precise alternating cellular pattern in the inner ear by coordinated hopping intercalations and delaminations, *Sci. Adv.* **9**, eadd2157 (2023).
- [36] See Supplemental Material at <http://link.aps.org/supplemental/10.1103/PRXLife.1.013001> for details.
- [37] A. Saraswathibhatla, S. Henkes, E. E. Galles, R. Sknepnek, and J. Notbohm, Coordinated tractions increase the size of a collectively moving pack in a cell monolayer, *Extreme Mech. Lett.* **48**, 101438 (2021).
- [38] D. L. Barton, S. Henkes, C. J. Weijer, and R. Sknepnek, Active vertex model for cell-resolution description of epithelial tissue mechanics, *PLoS Comput. Biol.* **13**, e1005569 (2017).
- [39] T. H. Tan, J. Liu, P. W. Miller, M. Tekant, J. Dunkel, and N. Fakhri, Topological turbulence in the membrane of a living cell, *Nat. Phys.* **16**, 657 (2020).
- [40] J.-Y. Tinevez, N. Perry, J. Schindelin, G. M. Hoopes, G. D. Reynolds, E. Laplantine, S. Y. Bednarek, S. L. Shorte, and K. W. Eliceiri, TrackMate: An open and extensible platform for single-particle tracking, *Methods* **115**, 80 (2017).
- [41] D. B. Allan, T. Caswell, N. C. Keim, C. M. van der Wel, and R. W. Verweij, soft-matter/trackpy: Trackpy version 0.5.0, 2021.
- [42] J. A. Mitchel, A. Das, M. J. O'Sullivan, I. T. Stancil, S. J. DeCamp, S. Koehler, O. H. Ocaña, J. P. Butler, J. J. Fredberg, M. A. Nieto *et al.*, In primary airway epithelial cells, the unjamming transition is distinct from the epithelial-to-mesenchymal transition, *Nat. Commun.* **11**, 5053 (2020).
- [43] E. Hannezo and C.-P. Heisenberg, Rigidity transitions in development and disease, *Trends Cell Biol.* **32**, 433 (2022).
- [44] P. Sahu, D. M. Sussman, M. Rübsam, A. F. Mertz, V. Horsley, E. R. Dufresne, C. M. Niessen, M. C. Marchetti, M. L. Manning, and J. M. Schwarz, Small-scale demixing in confluent biological tissues, *Soft Matter* **16**, 3325 (2020).
- [45] M. Krajnc, Solid-fluid transition and cell sorting in epithelia with junctional tension fluctuations, *Soft Matter* **16**, 3209 (2020).
- [46] A. Yanagida, E. Corujo-Simon, C. K. Revell, P. Sahu, G. G. Stirparo, I. M. Aspalter, A. K. Winkel, R. Peters, H. De Belly, D. A. D. Cassani *et al.*, Cell surface fluctuations regulate early embryonic lineage sorting, *Cell* **185**, 777 (2022).
- [47] J.-M. Yang, S. Bhattacharya, H. West-Foyle, C.-F. Hung, T.-C. Wu, P. A. Iglesias, and C.-H. Huang, Integrating chemical and mechanical signals through dynamic coupling between cellular protrusions and pulsed ERK activation, *Nat. Commun.* **9**, 4673 (2018).
- [48] E. Moreno, L. Valon, F. Levillayer, and R. Levayer, Competition for space induces cell elimination through compaction-driven ERK downregulation, *Curr. Biol.* **29**, 23 (2019).
- [49] A. G. Goglia, M. Z. Wilson, S. G. Jena, J. Silbert, L. P. Basta, D. Devenport, and J. E. Toettcher, A live-cell screen for altered Erk dynamics reveals principles of proliferative control, *Cell Syst.* **10**, 240 (2020).
- [50] H. Lavoie, J. Gagnon, and M. Therrien, ERK signaling: A master regulator of cell behaviour, life and fate, *Nat. Rev. Mol. Cell Biol.* **21**, 607 (2020).
- [51] H. De Belly, A. Stubb, A. Yanagida, C. Labouesse, P. H. Jones, E. K. Paluch, and K. J. Chalut, Membrane tension gates ERK-mediated regulation of pluripotent cell fate, *Cell Stem Cell* **28**, 273 (2021).
- [52] P. A. Gagliardi, M. Dobrzyński, M.-A. Jacques, C. Dessauges, P. Ender, Y. Blum, R. M. Hughes, A. R. Cohen, and O. Pertz, Collective ERK/Akt activity waves orchestrate epithelial homeostasis by driving apoptosis-induced survival, *Dev. Cell* **56**, 1712 (2021).
- [53] L. Valon, A. Davidović, F. Levillayer, A. Villars, M. Chouly, F. Cerqueira-Campos, and R. Levayer, Robustness of epithelial sealing is an emerging property of local ERK feedback driven by cell elimination, *Dev. Cell* **56**, 1700 (2021).
- [54] M. F. Simsek, A. S. Chandel, D. Saparov, O. Q. H. Zinani, N. Clason, and E. M. Özbudak, Periodic inhibition of Erk activity drives sequential somite segmentation, *Nature (London)* **613**, 153 (2023).
- [55] K. W. Pond, J. M. Morris, O. Alkhimenok, R. P. Varghese, C. R. Cabel, N. A. Ellis, J. Chakrabarti, Y. Zavros, J. L. Merchant, C. A. Thorne *et al.*, Live-cell imaging in human colonic monolayers reveals ERK waves limit the stem cell compartment to maintain epithelial homeostasis, *eLife* **11**, e78837 (2022).

- [56] Y. Zhang and É. Fodor, Pulsating active matter, [arXiv:2208.06831](https://arxiv.org/abs/2208.06831).
- [57] S. Monfared, G. Ravichandran, J. E. Andrade, and A. Doostmohammadi, Stress percolation criticality of glass to fluid transition in active cell layers, [arXiv:2210.08112](https://arxiv.org/abs/2210.08112).
- [58] T. Yamamoto, D. M. Sussman, T. Shibata, and M. L. Manning, Non-monotonic fluidization generated by fluctuating edge tensions in confluent tissues, *Soft Matter* **18**, 2168 (2022).
- [59] D. Pinheiro, R. Kardos, É. Hannezo, and C.-P. Heisenberg, Morphogen gradient orchestrates pattern-preserving tissue morphogenesis via motility-driven unjamming, *Nat. Phys.* **18**, 1482 (2022).
- [60] L. Bocanegra-Moreno, A. Singh, E. Hannezo, M. Zagorski, and A. Kicheva, Cell cycle dynamics control fluidity of the developing mouse neuroepithelium, *Nat. Phys.* **19**, 1050 (2023).
- [61] T. B. Saw, A. Doostmohammadi, V. Nier, L. Kocgozlu, S. Thampi, Y. Toyama, P. Marcq, C. T. Lim, J. M. Yeomans, and B. Ladoux, Topological defects in epithelia govern cell death and extrusion, *Nature (London)* **544**, 212 (2017).
- [62] R. Mueller, J. M. Yeomans, and A. Doostmohammadi, Emergence of Active Nematic Behavior in Monolayers of Isotropic Cells, *Phys. Rev. Lett.* **122**, 048004 (2019).
- [63] J. Eckert, B. Ladoux, L. Giomi, and T. Schmidt, Hexanematic crossover in epithelial monolayers depends on cell adhesion and cell density, doi:[10.1101/2022.10.07.511294](https://doi.org/10.1101/2022.10.07.511294).
- [64] D.-Q. Zhang, P.-C. Chen, Z.-Y. Li, R. Zhang, and B. Li, Topological defect-mediated morphodynamics of active-active interfaces, *Proc. Natl. Acad. Sci. USA* **119**, e2122494119 (2022).
- [65] R. Thiagarajan, A. Bhat, G. Salbreux, M. M. Inamdar, and D. Riveline, Pulsations and flows in tissues as two collective dynamics with simple cellular rules, *iScience* **25**, 105053 (2022).
- [66] M. F. Staddon, K. E. Cavanaugh, E. M. Munro, M. L. Gardel, and S. Banerjee, Mechanosensitive junction remodeling promotes robust epithelial morphogenesis, *Biophys. J.* **117**, 1739 (2019).
- [67] K. E. Cavanaugh, M. F. Staddon, T. A. Chmiel, R. Harmon, S. Budnar, S. Banerjee, M. L. Gardel *et al.*, Force-dependent intercellular adhesion strengthening underlies asymmetric adherens junction contraction, *Curr. Biol.* **32**, 1986 (2022).
- [68] L. D. Hayden, K. D. Poss, A. De Simone, and S. D. Talia, Mathematical modeling of Erk activity waves in regenerating zebrafish scales, *Biophys. J.* **120**, 4287 (2021).
- [69] https://github.com/DBoocock/erk_waves